Multi-Objective Optimization Design of Cable Driven Parallel Robot Based on Aircraft Spraying

Zonghui Yang
College of Information and Control Engineering
Jilin Institute of Chemical Technology
Jilin, China
2717688181@qq.com

Ting Liu*
College of Aerospace Engineering
Jilin Institute of Chemical Technology
Jilin, China
liuting@jlict.edu.cn

Sen Jiao
College of Information and Control Engineering
Jilin Institute of Chemical Technology
Jilin, China
jiaosen@jlict.edu.cn

Xudong Chang
College of Information and Control Engineering
Jilin Institute of Chemical Technology
Jilin, China
changxudong1@jlict.edu.cn

2024 9th International Conference on Automation, Control and Robotics Engineering (CACRE) | 979-8-3503-5030-2/24/$31.00 ©2024 IEEE | DOI: 10.1109/CACRE62362.2024.10635071

***Abstract*—This article focuses on the cable driven parallel robot for aircraft spraying. Based on a multi-objective optimization model, the performance of the cable driven parallel robot (CDPR) is optimized using Prairie Dogs optimization algorithm. Firstly, a static model of 8-cable 6-degree-of-freedom CDPR suitable for aircraft spraying was established, and corresponding evaluation indicators were designed for four performance indicators: workspace, average stiffness, stiffness fluctuation, and flexibility. Establish a multi-objective optimization model by processing performance indicators and solve it using the Prairie Dogs optimization algorithm. The final results indicate that the groundhog optimization algorithm based on multi-objective optimization design has a good effect on the performance optimization of CDPR, providing important reference for the design and optimization of aircraft spraying robots. This study has important theoretical and practical significance in the field of aircraft spraying robots, providing new ideas and methods for optimizing robot performance, and has certain guiding significance for engineering practice.**

Keywords—Cable driven parallel robot, multi-objective optimization design, average stiffness, workspace, stiffness fluctuation, flexibility, Prairie Dogs optimization algorithm

I. INTRODUCTION

Cable driven parallel robot (CDPR) is a type of parallel robot that achieves spatial motion of end effectors through coordinated retraction and release of multiple flexible cables[1]. The cable parallel robot uses flexible cables as the driving element, making it highly flexible and flexible. At the same time, it has the characteristics of simple structure, large workspace, and high-speed operation, and is widely used in transportation[2], assembly[3], flight experiments[4], aviation maintenance[5] and other fields. However, in aircraft spraying and other work, the influence of inherent properties on CDPR motion control and work efficiency is often significant and cannot be ignored, so the performance of CDPR urgently needs to be optimized.

In terms of performance optimization of CDPR, Yaqing Zheng et al.[6] considered the influence of the self-weight of the rope and derived a general expression for the static stiffness of a 4-cable 6-degree-of-freedom CDPR based on a catenary. They also optimized the weak links of the static stiffness of a 4-cable 6-degree-of-freedom unconstrained CDPR using least squares support vector machine generalization. Gueners et al.[7] aimed to maximize the stiffness of additive manufactured CDPR and optimized the anchor position of the robot. Hamed et al.[8] improved the translational stiffness of the CDPR end effector by optimizing the cable force distribution. Weiwei Shang et al.[9] considered three performance indicators: time, energy, and stiffness during the CDPR motion process, and used intelligent optimization algorithms to achieve multi-objective dynamic trajectory planning for CDPR. Hongjun Xiao et al.[10] optimized the workspace area, overall stiffness index, and global dexterity coefficient of parallel robots based on genetic algorithm and ideal point method, and the optimization results were relatively balanced. Xuechao Duan et al.[11] established a structural optimization model with the dexterity of a 6-degree-of-freedom Stewart parallel robot as the objective function, and the design space, the ratio of the maximum and minimum lengths of each leg, and the maximum swing angles of the Hooke and ball joints as constraints. They designed the M Metropolis genetic algorithm and used it to solve the CDPR structural optimization problem. By comparing the results obtained with the standard genetic algorithm, the effectiveness and superiority of the M Metropolis genetic algorithm in CDPR structural optimization design were confirmed. Lorenzo et al.[12] focused their research on reconfigurable cable driven parallel robots and proposed a method based on optimal reconstruction strategy. The Dijkstra algorithm was used for optimization in the study, which provides useful ideas and methods for the design and control of reconfigurable cable driven parallel robots, and is of great significance for the progress in this field.

Previous research has mainly focused on optimizing and studying the support mechanism properties of CDPR, as well as using existing optimization algorithms to optimize the performance of CDPR. For aircraft spraying robots, in addition to ensuring a large workspace, the end effector mechanism also needs to have high flexibility, and good and stable stiffness to ensure the accuracy of spraying work.

This article also established a static model of 8-cable 6-degree of freedom CPDPR suitable for aircraft spraying, and designed corresponding evaluation indicators for four performance indicators, including workspace, average stiffness, stiffness fluctuation, and flexibility. Finally, the optimization solution was obtained using the groundhog optimization algorithm, and satisfactory results were obtained.

II. INSTITUTIONAL DESCRIPTION

This article designs a CDPR model suitable for aircraft spraying, with a configuration prototype shown in Figure 1. The CDPR consists of a support mechanism (static platform), 8 drivers, 8 ropes, pulleys, and a central mobile spraying robotic arm (moving platform). Below is a model of the aircraft to be sprayed. Eight drivers are installed at the four corners below the support mechanism, and each rope is connected to the moving platform through the driver, pulley group, and cable outlet point. The position of the cable outlet point can be changed according to needs. The moving platform has 6 degrees of freedom and can move freely in space. The movement of the moving platform is controlled by the driver pulling the rope. When the moving platform reaches the designated position, the spraying robot completes the designated spraying task.

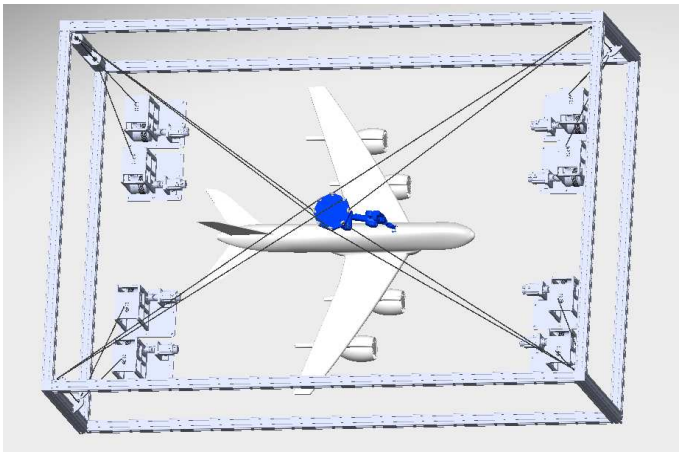

Fig. 1. Cable parallel spraying robot

III. STATIC ANALYSIS

For the convenience of theoretical analysis, the CDPR model designed in this article is simplified according to the structural characteristics as shown in Figure 2. The static platform is simplified as a rectangle, the dynamic platform is simplified as a regular octagon, A_i is the exit point, and B_i is the connection point between the rope and the dynamic platform. Establish the global coordinate system $O-XYZ$ and the local coordinate system $O'-X'Y'Z'$ as shown in Figure 3, with their origin located at the center of the circumscribed circles of the stationary and moving platforms, respectively. The z -axis is perpendicular to the ground downwards, and the radii of their circumscribed circles are r_a and r_b, respectively. The position vectors of each exit point on the static platform are represented as:

$$A_i = [r_a \cos\varphi_i, r_a \sin\varphi_i, 0] \tag{1}$$

$$\varphi_i = \frac{\pi}{4}\left[i + \frac{(-1)^{i+1}-1}{2}\right] + (-1)^i \frac{\theta}{2} \tag{2}$$

Where φ_i represents the index point, φ_i=1, 2, 3,..., 8; For the convenience of calculation, define $A_i = A_{i-4}$; The position vectors of each hinge point on the moving platform are represented as:

$$B_i = [r_b \cos\psi_i, r_b \sin\psi_i, 0] \tag{3}$$

$$\psi_i = \frac{\pi}{4}[i-1] \tag{4}$$

Where ψ_i represents the index point，i=1，2，3，…，8；

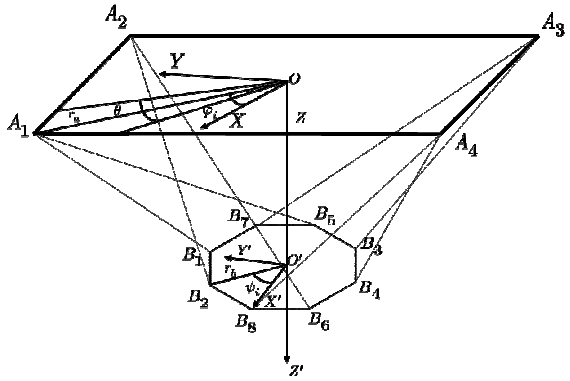

Fig. 2. Schematic diagram of aircraft spraying mechanism

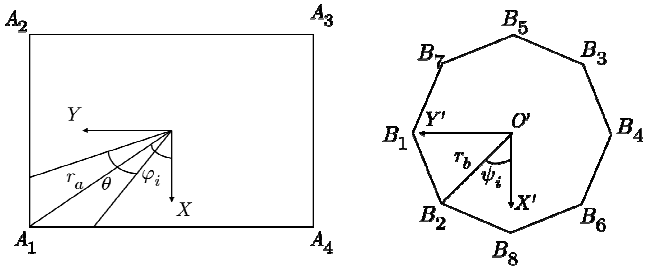

Fig. 3. Schematic diagram of the location of the retrieval point and connection point

The position vector O' of the moving platform is represented as $T_{O'} = ({}^{O}x_{O'} \quad {}^{O}y_{O'} \quad {}^{O}z_{O'})^T$ under O, and the Euler angle $(\alpha \quad \beta \quad \gamma)^T$ is used to represent the attitude of the moving platform. The pose of the moving platform is represented in the global coordinate system as:

$$X = ({}^{O}x_{O'} \quad {}^{O}y_{O'} \quad {}^{O}z_{O'} \quad \alpha \quad \beta \quad \gamma)^T \tag{5}$$

As shown in Figure 2, any rope in the global coordinate system is represented as:

$${}^{O}L_i = {}^{O}R_{O'}{}^{O'}B_i + {}^{O}T_{O'} - {}^{O}A_i \tag{6}$$

Therefore, the length of the rope is expressed as:

$$l_i = \| {}^{O}L_i \|_2 \tag{7}$$

Where ${}^{O}A_i$ and ${}^{O'}B_i$ are the position vectors of points A_i and B_i in the global coordinate system; ${}^{O}R_{O'}$ is the rotation matrix of the moving coordinate system relative to the stationary coordinate system, expressed as:

$${}^{O}R_{O'} = \begin{bmatrix} c\alpha c\beta c\gamma - s\alpha s\gamma & -c\alpha c\beta s\gamma - s\alpha c\gamma & c\alpha s\beta \\ s\alpha c\beta c\gamma + c\alpha s\gamma & -s\alpha c\beta s\gamma + c\alpha c\gamma & s\alpha s\beta \\ -s\alpha c\beta c\gamma & s\beta s\gamma & c\beta \end{bmatrix} \tag{8}$$

Where $c = \cos$, $s = \sin$.

The static equilibrium equation of the mechanism is:

$$\begin{cases} \sum_{i=1}^{8} T_i + F = 0 \\ \sum_{i=1}^{8} r_i \times T_i + M = 0 \end{cases} \tag{9}$$

Where $T_i = t_i u_i$, t_i is the tensile force of the i rope, and $u_i = \dfrac{{}^{O}L_i}{l_i}$ is the unit vector of the i rope along the direction of the rope; r_i is the vector relative to O' at the connection point between the rope and the moving platform; F is the external force acting on the moving platform; M is the external torque acting on the moving platform. By organizing the above formulas, it can be concluded that:

$$\begin{pmatrix} u_1 & u_2 & \cdots & u_8 \\ r_1 \times u_1 & r_2 \times u_2 & \cdots & r_8 \times u_8 \end{pmatrix} (t_1 \ t_2 \cdots \ t_8)^T = W \tag{10}$$

Simplify the above formula as follows:

$$JT = W \tag{11}$$

Where $J \in R^{8\times 8}$ is the Jacobian matrix of the system; $W = -(F \ \ M)^T$ is the external torque of the organization's management, which is the quality of the dynamic platform in this article.

IV. Static stiffness model

The stiffness of CDPR is an important criterion for measuring the performance of the mechanism. The static stiffness of CDPR at any position in the workspace in this article can be represented by the stiffness matrix K, and the following relationship is satisfied:

$$K = -\frac{dF}{dX} = -\frac{dJ}{dX}T - J\frac{dT}{dX} = K_1 + K_2 \tag{12}$$

The stiffness matrix K can be divided into two parts: the positional stiffness K_1 of the system and the positional stiffness K_2 of the rope.

A. Platform pose stiffness

The pose stiffness K_1 of the system is related to the platform pose change, and K_1 satisfies:

$$K_1 = -\frac{dJ}{dX}T = -\frac{d}{dX}\begin{pmatrix} u_1 & u_2 & \cdots & u_8 \\ r_1 \times u_1 & r_2 \times u_2 & \cdots & r_8 \times u_8 \end{pmatrix} T = \sum_{i=1}^{n}\left[-\frac{d}{dX}\begin{pmatrix} u \\ r \times u_i \end{pmatrix}_i T_i \right] \tag{13}$$

Where $-\dfrac{d}{dX}\begin{pmatrix} u \\ r \times u_i \end{pmatrix}_i$ is a matrix of 6×6 and satisfies:

$$-\frac{d}{dX}\begin{pmatrix} u \\ r \times u_i \end{pmatrix}_i = \begin{bmatrix} -\dfrac{du}{dx} & -\dfrac{du}{d\omega} \\ -r \times \dfrac{du}{dx} - \dfrac{dr}{dx} \times u & -r \times \dfrac{du}{d\omega} - \dfrac{dr}{d\omega} \times u \end{bmatrix}_i \tag{14}$$

Among them, each sub matrix can be further derived. When the CDPR cable undergoes translational displacement dx, the cable tension vector T becomes T', the corresponding u becomes u', and the increment is du, then there is

$$du = u' - u = \frac{T'}{|T'|} - \frac{T}{|T|} = \frac{1}{L_c}\begin{bmatrix} {u_x}^2 - 1 & u_x u_y & u_x u_z \\ & {u_y}^2 - 1 & u_y u_z \\ & & {u_z}^2 - 1 \end{bmatrix} dx \tag{15}$$

Among them, L_c is the modulus of CDPR rope vector T, which can be approximated as the length of the rope. When the point of action of the cable force is displaced and the increment is defined as $dr = dx = d\omega \times r$, it can be obtained that:

$$-\frac{du}{d\omega} = -\frac{du}{d\omega \times r}\frac{d\omega \times r}{d\omega} = -\frac{du}{dx}(I \times r) = -\left(r^T \times \frac{du}{dx}\right) I \tag{16}$$

Where I is the unit matrix, and the other terms are:

$$-\frac{dr}{dx} \times u = -I \times u = \begin{bmatrix} 0 & -u_z & u_y \\ u_z & 0 & -u_x \\ -u_y & u_x & 0 \end{bmatrix} \tag{17}$$

$$-\frac{dr}{d\omega} \times u = \frac{d\omega \times r}{d\omega} \times u = -(I \times r) \times u \tag{18}$$

$$-r \times \frac{du}{d\omega} = RDU \tag{19}$$

The detailed derivation of formulas A $-\left(r^T \times \frac{du}{dx}\right) I$, $-(I \times r) \times u$, and RDU can be found in Appendix Formulas [43], [44], and [45].

From the above formula, it can be concluded that:

$$K_1 = \begin{bmatrix} -\frac{du}{dx} & -\frac{du}{d\omega} \\ -r \times \frac{du}{dx} - \frac{dr}{dx} \times u & -r \times \frac{du}{d\omega} - \frac{dr}{d\omega} \times u \end{bmatrix}_i T_i \quad (20)$$

B. Positional stiffness

The positional stiffness K_2 of the rope depends on the properties of the rope itself, and is mainly influenced by the elastic modulus and cross-section. In general, the self-weight of the cable can be ignored, while the tension of the cable is mainly generated by changes in the cable configuration. Therefore:

$$K_2 = -J \frac{\partial T}{\partial l} \frac{\partial l}{\partial X} \quad (21)$$

Based on the elastic modulus E, cross-sectional area A, and cable length l of the rope:

$$\partial t_i = \frac{E_i A_i}{l_{io}} \partial l_i \quad (22)$$

Where l_{io} is the length before cable deformation:

$$\frac{\partial T}{\partial l} = \mathrm{diag}\left(\frac{E_1 A_1}{l_{1o}}, \ \cdots \ \frac{E_8 A_8}{l_{8o}}\right) \quad (23)$$

From $\frac{\partial l}{\partial x} = -J^T$:

$$K_2 = J \, \mathrm{diag}\left(\frac{E_1 A_1}{l_{1o}}, \ \cdots \ \frac{E_8 A_8}{l_{8o}}\right) J^T \quad (24)$$

From this, the stiffness $K = K_1 + K_2$ of the system is obtained.

V. Multi-objective optimization design

A. Workplace metrics

When only considering the gravity effect of the end effector, CDPR can maintain a stationary set of positions and postures. The workspace is an important indicator used to describe the performance of CDPR, where factors such as the size, shape, and accessibility of the workspace directly affect the performance of CDPR. The CDPR workspace in this article is represented as:

$$W_s = V \quad (25)$$

Where V is the volume of the workspace. In this article, the exhaustive method is used to search for the workspace of the mechanism, and the number of scattered points obtained is approximately V.

B. Rigidity performance indicators

For CDPR, stiffness is an important performance indicator that directly affects the positioning accuracy and work stability of the robot. Higher stiffness can reduce the deformation of the robot under force, improve its positioning accuracy and work stability, and better meet the needs of precision operation and control. The stiffness index of CDPR designed in this article selects its average value, which is defined as:

$$\bar{K} = \frac{1}{V} \int_V \| K \|_2 \, dV \quad (26)$$

Due to the fact that the workspace V in this article is scattered, the average stiffness $\bar{K}$ is discretized as:

$$\bar{K} = \frac{1}{N} \sum_{i=1}^{N} \| K_i \|_2 \quad (27)$$

Where N is the number of discrete points in the workspace.

C. Rigidity fluctuation index

The stiffness fluctuation of CDPR is crucial for this system, as higher stiffness fluctuation can lead to increased positioning error, unstable operation, decreased control accuracy, and even shorten the service life of CDPR, increasing maintenance costs. Variance and mean absolute deviation are important indicators for measuring volatility. The former is more sensitive to outliers, while the latter is relatively insensitive to outliers. Therefore, this article selects the mean absolute deviation of stiffness as the indicator for measuring stiffness volatility, defined as:

$$M_{AD} = \frac{1}{V} \int_V \left| \| K \|_2 - \bar{K} \right| dV \quad (28)$$

Discretize M_{AD} and adjust it to:

$$\bar{M}_{AD} = 1 - \frac{1}{N} \sum_{i=1}^{N} \left| \| K_i \|_2 - \bar{K} \right| \quad (29)$$

Where N is the number of discrete points in the workspace, and $\bar{K}$ is the average stiffness.

D. Flexibility performance indicators

Flexibility determines the range of motion and degrees of freedom of a robot, enabling it to adapt to different working environments and perform diverse tasks. A highly flexible robot system can quickly and effectively adapt to different work scenarios, improving work efficiency and flexibility. For complex tasks such as aircraft spraying, the end effector of CDPR needs to have high flexibility to ensure the accuracy and reliability of the spraying robotic arm's movements. In CDPR, the reciprocal of the condition number of the Jacobian matrix is considered an important flexibility indicator[13]. The closer the reciprocal of the condition number is to 1, the better the kinematic performance and flexibility of the robot in a specific working position. Then define $m(D)$ as:

$$m(D)=\|D\|_2\cdot\|D^{-1}\|_2=\frac{\sigma_{\max}(D)}{\sigma_{\min}(D)}\geqslant 1 \tag{30}$$

Where $D=JJ^T$, $\|D\|_2$ represents the 2-norm of D , while $\sigma_{\max}(D)$ and $\sigma_{\min}(D)$ denote the maximum and minimum eigenvalues of D . The flexibility c is defined as follows:

$$c=\frac{1}{V}\int_V\frac{1}{m(D)}dV \tag{31}$$

Discretize c to:

$$\overline{c}=\frac{1}{N}\sum_{i=1}^{N}\frac{1}{m(D)} \tag{32}$$

Obviously, the flexibility of CDPR is between 0 and 1. When $\overline{c}$ approaches 1, the higher the flexibility of CDPR. Conversely, when $\overline{c}$ approaches 0, the lower the flexibility of CDPR.

E. Objective Function Design

The workspace, average stiffness, stiffness fluctuation, and flexibility are important indicators for CDPR's multi-objective optimization, and for multi-objective optimization attempts, they are transformed into single objective optimization. This article adopts the multi-objective addition and subtraction method in optimization theory, and defines the multi-objective optimization model as:

$$\begin{cases}\min & F=-W_s(d)-\overline{K}(d)-\overline{M}_{AD}(d)-\overline{c}(d)\\ s.t. & d_{i\min}<d_i<d_{i\max}\qquad i=1,\cdots,n\end{cases} \tag{33}$$

Where $d=\{d_1,\cdots,d_n\}$ is the set of constraint functions. In the optimization process of this article, the constraint function selects the influence factor θ of the index point and the size radius r_b of the moving platform; W_s , $\overline{K}$, $\overline{M}_{AD}$, and $\overline{c}$ represent workspace, average stiffness, stiffness fluctuation, and flexibility, respectively.

In multi-objective optimization, normalization can unify the dimensions and ranges of different objective functions, making them comparable and avoiding optimization algorithms leaning towards objective functions with larger value ranges. And normalization can improve the convergence speed of optimization algorithms, making them faster in finding global or partial Pareto optimal solutions. By normalization, the weight selection of different objective functions becomes more intuitive and simplified, which helps to improve the interpretability of the results. This article establishes a normalized model for each objective:

$$f=\frac{f_i-f_{\min}}{f_{\max}-f_{\min}} \tag{34}$$

Where f is the normalized objective function, while f_i represents the objective function. $f_{\min}$ and $f_{\max}$ represent the minimum and maximum possible values of the objective function

F. Optimization Algorithm for Prairie Dogs

The basic idea of PDO[14] is to divide the behavior of Prairie Dogs into two stages. The first stage is the global exploration stage, which is divided into two behavioral patterns: food search behavior and cave construction behavior; The second stage is the local development stage, which is divided into two behavioral patterns: response behavior to food source signals and predator signals.

Prairie Dogs search for new sources of food within their nests by individuals, and this behavior is expressed as:

$$\begin{aligned}PD_{i+1,\ j+1}=&GBest_{ij}-eCBest_{ij}\times\rho-\\&CPD_{i,j}\times Levy(n)\ \forall iter<\frac{Max_{iter}}{4}\end{aligned} \tag{35}$$

Prairie Dogs will continuously dig new burrows, which is represented by:

$$\begin{aligned}PD_{i+1,\ j+1}=&GBest_{ij}\times rPD\times DS\times\\&Levy(n)\ \forall\frac{Max_{iter}}{4}\leqslant iter<\frac{Max_{iter}}{2}\end{aligned} \tag{36}$$

Where $PD_{i,j}$ is the individual's location, $GBest_{ij}$ is the current global optimal solution, $Levy(n)$ is the standard Levi's function, ρ is the food source alarm, rPD is the location of the random solution, $eCBest_{i,j}$, $CPD_{i,j}$ and DS are represented as follows:

$$eCBest_{i,j}=GBest_{ij}\times\Delta+\frac{PD_{i,j}\times mean(PD_{m,n})}{GBest_{i,j}\times(UB_j-LB_j)+\Delta} \tag{37}$$

Where $eCBest_{i,j}$ evaluates the effectiveness of the currently obtained optimal solution, UB and LB represent the upper and lower limits of the boundary, and Δ represents the differences between individual Prairie Dogs.

$CPD_{i,j}$ is the cumulative effect in the population of Prairie Dogs, expressed as:

$$CPD_{i,j}=\frac{GBest_{i,j}-CPD_{i,j}}{GBest_{i,j}+\Delta} \tag{38}$$

DS is the digging intensity of a small team, which depends on the quality of the food source, expressed as:

$$DS=1.5\times r\times\left(1-\frac{iter}{Max_{iter}}\right)^{\left(2\frac{iter}{Max_{iter}}\right)} \tag{39}$$

In the development stage of Prairie Dogs, the first sound can transmit the source and quality of food. When an individual discovers a high-quality food source, the remaining individuals will gather at the sound source location to meet their food needs. The position update model for this situation is represented as:

$$PD_{i+1,j+1} = GBest_{i,j} - eCBest_{i,j} \times \varepsilon - CPD_{i,j} \times rand \forall \frac{Max_{iter}}{2} iter < \frac{Max_{iter}}{3} \quad (40)$$

The second type of sound serves as a warning to the existence of predators of the same species. The Prairie Dogs on the predator's path will hide, and the position update model for this situation is represented as:

$$PD_{i+1,j+1} = GBest_{i,j} \times PE \times rand \forall \frac{3Max_{iter}}{4} < iter < Max_{iter} \quad (41)$$

Where $rand$ is a random number in $[0,1]$, and PE is the predator effect expressed as:

$$PE = 1.5 \times \left(1 - \frac{iter}{Max_{iter}}\right)^{\left(2\frac{iter}{Max_{iter}}\right)} \quad (42)$$

G. *The influence of exit point and moving platform size on CDPR*

The aircraft spraying CDPR designed in this article often needs to maintain a fixed orientation for the moving platform to facilitate research. Due to the fact that the rope can only withstand tension and cannot withstand pressure, it is necessary to ensure that the cable tension in any position must be greater than 0. For the convenience of research, it is assumed that the moving platform is in a horizontal state. Therefore, Therefore, the rotation angle is defined as $\alpha = \beta = \gamma = 0$,the relevant parameters of mechanisms are shown in Table I:

TABLE I. CDPR INSTITUTION PARAMETER TABLE

Parameter Name	Numerical values and units
Static platform radius r_a	$4m$
The distance h between the ground and the static platform	$2m$
Mass of moving platform m	$10kg$
The nominal radius r of the rope r	$0.6mm$
The cross-sectional area r of the rope A	$1.131mm^2$
The elastic modulus E of the rope	$28GPa$
Gravitational acceleration g	$9.8m \cdot s^{-2}$

As shown in Figure 4, the workspace decreases with the increase of θ angle. When θ angle is 45 ° and 15 °, the workspace does not change much with the increase of r_b. However, when θ angle is 0 °, the workspace decreases overall with the increase of r_b. However, when θ angle is 30 °, the workspace increases overall with the increase of r_b. The average stiffness and the average absolute deviation of global stiffness will increase with the increase of θ and r_b; The flexibility of CDPR will decrease with the increase of θ and r_b.

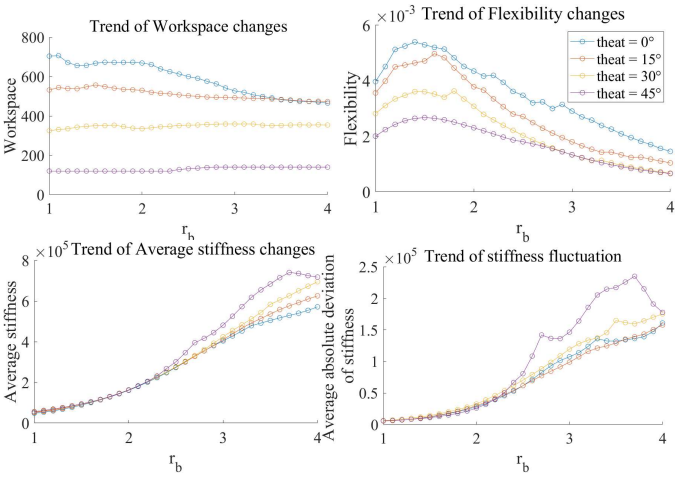

Fig. 4. Trends in CDPR performance indicators

VI. MULTI OBJECTIVE OPTIMIZATION OF PDO ALGORITHM FOR SOLVING CDPR

By normalizing the above performance indicators, the objective function $F \in [-4, 0]$ is obtained, and the smaller the F value, the better the CDPR performance indicator. The PDO algorithm was used to solve the multi-objective optimization model designed in this paper, and the solution space was obtained as a non convex solution space as shown in Figure 5. The optimal solution was -2.7984, which is r_b=2.335m,θ=0 °.

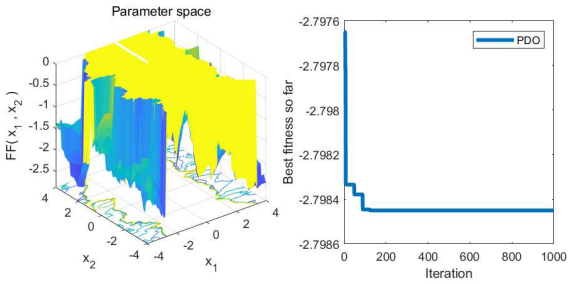

Fig. 5. Solution space and optimal solution

Before optimization, the initial state was r_b=2m and θ=30 °. The differences in workspace, average stiffness, stiffness fluctuation, and flexibility before and after optimization are shown in Table II. After optimization, the workspace increased by 100%, the average stiffness increased by 89.1%, while stiffness fluctuation decreased by 18.7% and flexibility increased by 82.0%. After calculation, the objective function has decreased by 42.5% compared to before optimization, and the overall optimization effect is significant.

TABLE II. COMPARISON OF CDPR PERFORMANCE BEFORE AND AFTER OPTIMIZATION

Performance index	Before Optimization	After Optimization
Workspace	0.4444	0.8889
Stiffness	0.1453	0.2748

Performance index	Before Optimization	After Optimization
Rigidity Fluctuation	0.8605	0.7
Flexibility	0.5138	0.9347

VII. CONCLUSION

This article designs an aircraft spraying CDPR with 8-cable 6-degree-of-freedom. Based on static analysis, a CDPR static model is established, and four performance optimization indicators are proposed, including workspace, stiffness, stiffness fluctuation, and flexibility. After normalizing the optimization objectives, a multi-objective optimization model is established. Finally, the model is optimized based on the Prairie Dogs optimization algorithm, and compared with the performance indicators before optimization. The optimization effect is obvious, and the CDPR performance is significantly improved.

REFERENCES

[1] Qian S ,Zi B ,Shang W , et al.A Review on Cable-driven Parallel Robots [J].Chinese Journal of Mechanical Engineering,2018,31(04):37-47.

[2] Cristian Calderón.A Simulation Study of a Planar Cable-Driven Parallel Robot to Transport Supplies for Patients with Contagious Diseases in He alth Care Centers[J].Robotics, 2021, 10.DOI:10.3390/robotics10040111.

[3] Martin A , Caro S , Cardou P .Design of a Cable-Driven Parallel Robot with Grasping Device[C]//CIRP Design Conference.2018.

[4] Wu J ,Sun Y ,Yue H , et al.Design and Optimization of UAV Aerial Rec overy System Based on Cable-Driven Parallel Robot[J].Biomimetics,20 24,9(2):.

[5] Nguyen D Q , Gouttefarde M .Study of Reconfigurable Suspended Cabl e-Driven Parallel Robots for Airplane Maintenance[J].IEEE, 2014:1682-1689.DOI:10.1109/IROS.2014.6942781.

[6] Zheng Yaqing, Jiang Xiaoling. Static stiffness analysis and optimization of a 6-degree-of-freedom underconstrained parallel robot with four rope traction based on least squares support vector machine [J]. Journal of Me chanical Engineering, 2012,48(13):49-55.

[7] Gueners,D.,Chanal,H.,and Bouzgarrou, B. C.,2020,“Stiffness Optimizati on of a Cable Driven Parallel Robot for Additive Manufacturing,” 2020 IEEE International Conference on Robotics and Automation (ICRA),Par is,France,May 31–Aug.31,IEEE,pp.843–849.

[8] Jamshidifar H , Khajepour A , Fidan B ,et al.Kinematically-Constrained Redundant Cable-Driven Parallel Robots: Modeling, Redundancy Analy sis, and Stiffness Optimization[J].IEEE/ASME Transactions on Mechatr onics, 2017.DOI:10.1109/TMECH.2016.2639053.

[9] Shang Weiwei, Dynamics Modeling, Control and Optimization of Parall el Robots. Anhui Province, University of Science and Technology of Ch ina,2012-05-01.

[10] Xiao Hongjun. Multi objective optimization of a planar fully constrained rope traction parallel robot [J]. Journal of Xi'an Engineering University, 2010,24(05):608-613+622.

[11] Duan Xuechao, Qiu Yuanying, Duan Baoyan. Structural optimization de sign of parallel robots based on Metropolis genetic algorithm [J]. Roboti cs,2006,(04):433-438.

[12] Gagliardini L ,Stéphane Caro, Gouttefarde M ,et al.A Reconfiguration St rategy for Reconfigurable Cable-Driven Parallel Robots[C]//IEEE Intern ational Conference on Robotics & Automation.IEEE, 2015.DOI:10.1109 /ICRA.2015.7139404.

[13] Zhou B, Li S, Zi B, et al. Multi-objective optimal design of a cable-drive n parallel robot based on an adaptive adjustment inertia weight particle s warm optimization algorithm[J]. Journal of Mechanical Design, 2023,14 5(8).

[14] Ezugwu A E, Agushaka J O, Abualigah L, et al. Prairie dog optimization algorithm[J]. Neural Computing and Applications, 2022, 34(22): 20017-20065.

APPENDIX

$$-\left(r^T\times\frac{du}{dx}\right)I=-\left(r\times\frac{du}{dx}\right)^T=\frac{1}{L_c}\begin{pmatrix} r_zu_xu_y-r_yu_xu_z & r_z(1-{u_x}^2)+r_xu_xu_z & -r_y(1-{u_x}^2)-r_xu_xu_y\\ -r_z(1-{u_y}^2)-r_yu_yu_z & r_xu_yu_z-r_zu_xu_y & r_x(1-{u_y}^2)+r_yu_xu_y\\ r_y(1-{u_z}^2)+r_zu_yu_z & -r_x(1-{u_z}^2)-r_zu_xu_z & r_yu_xu_z-r_xu_yu_z\end{pmatrix} \tag{43}$$

$$-(I\times r)\times u=-\left[(ru)-I(r\cdot u)\right]=\begin{bmatrix} r_yu_y+r_zu_z & -r_xu_y & -r_xu_z\\ -r_yu_x & r_xu_x+r_zu_z & -r_yu_z\\ -r_zu_x & -r_zu_y & r_xu_x+r_yu_y\end{bmatrix} \tag{44}$$

$$RDU=\frac{1}{L_c}\begin{bmatrix} {r_y}^2+{r_z}^2-(r_yu_z-r_zu_y)^2 & -r_xr_y-(r_yu_z-r_zu_y)(r_zu_x-r_xu_z) & -r_zr_x-(r_xu_y-r_yu_x)(r_yu_z-r_zu_y)\\ & {r_z}^2+{r_x}^2-(r_zu_x-r_xu_z)^2 & -r_zr_y-(r_xu_y-r_yu_x)(r_zu_x-r_xu_z)\\ & & {r_x}^2+{r_y}^2-(r_xu_y-r_yu_x)\end{bmatrix} \tag{45}$$

Where (ru) is the dyadic of vectors r and u, and $(r\cdot u)$ is the dot product of vectors r and u.